Quantitative Analysis to Find the Optimum Scale Range for Object Representations in Remote Sensing Images

Rasna A. Amit[a] and C. Krishna Mohan[b]
Indian Institute of Technology Hyderabad, Kandi, Sangareddy, Telangana, 502285, India

Keywords: Dynamic Kernel, Gaussian Mixture Model, MAP Adaptation, Object Representations, Remote Sensing Images, Scale Effect.

Abstract: Airport object surveillance using big data requires high temporal frequency remote sensing observations. However, the spatial heterogeneity and multi-scale, multi-resolution properties of images for airport surveillance tasks have led to severe data discrepancies. Consequently, artificial intelligence and deep learning algorithms suffer from accurate detections and effective scaling of remote sensing information. The quantification of intra-pixel differences may be enhanced by employing non-linear estimating algorithms to reduce its impact. An alternate strategy is to define scales that help minimize spatial and intra-pixel variability for various image processing tasks. This paper aims to demonstrate the effect of scale and resolution on object representations for airport surveillance using remote sensing images. In our method, we introduce dynamic kernel-based representations that aid in adapting the spatial variability and identify the optimum scale range for object representations for seamless airport surveillance. Airport images are captured at different spatial resolutions and feature representations are learned using large Gaussian Mixture Models (GMM). The object classification is done using a support vector machine and the optimum range is identified. Dynamic kernel GMMs can handle the disparities due to scale variations and image capturing by effectively preserving the local structure information, similarities, and changes in spatial contents globally for the same context. Our experiments indicate that the classification performance is better when both the first and second-order statistics for the Gaussian Mixture Models are used.

1 INTRODUCTION

Remote sensing technology has access to a large variety of real-time spatial data and is also known for its multi-scale multi-resolution properties that can be used for varied surveillance applications. Due to its rich information, these data are largely used to characterize remote sensing images aiding in multiple image processing tasks. These images, however, suffer from two major problems: greater scale sensitivity and information loss at coarse spatial resolutions. Hence, the need for enhancing feature representations and characterization of these images.

Scale sensitivity phenomena can be classified into scaling-effect and zoning-effect problems. Scale effects refer to the use of coarser or finer analysis units and zonal effects refer to the case of the problem by the division of the geographical area under study that may or may not be at the same spatial scale. The size of the units in spatial analysis directly determines the amount of information that needs to be included in the analysis, hence creating a scale effect. In general, scale is considered a function of resolution with a dependency on land-surface parameters and is considered a ‘basic problem in Geomorphometry’.

While most studies consider multi-scale multi-resolution models, the extraction of spatial patterns continues to rely on the single scale or single resolution. For example, standard grid sizes are used for most urban-oriented studies, where the sizes vary from 0.125m to 1m. Hence, selecting an appropriate scale when examining big data(geo-data) is deemed a challenge. Thus, scale sensitivity has been identified as a major challenge for object classification and detection for airport surveillance using remote sensing images.

Many researchers have confirmed the scale dependency of land-surface parameters and land-surface objects extensively in their works. Therefore, the factor of scale and resolution play a critical role in the

[a] https://orcid.org/0000-0003-4961-0291
[b] https://orcid.org/0000-0002-7316-0836

Amit, R. and Mohan, C.
Quantitative Analysis to Find the Optimum Scale Range for Object Representations in Remote Sensing Images.
DOI: 10.5220/0011599200003417
In *Proceedings of the 18th International Joint Conference on Computer Vision, Imaging and Computer Graphics Theory and Applications (VISIGRAPP 2023) - Volume 5: VISAPP*, pages 369-379
ISBN: 978-989-758-634-7; ISSN: 2184-4321

use of digital models. Also, the examination of the characteristics mainly the changing pattern as a function of scale and resolution is deemed critical for the study of images with an appropriate spatial resolution.

The high dimensional characteristics of remote sensing images introduce data variability and hence information loss. Hence, different feature representations are required to efficiently represent this data. Furthermore, due to the scarcity in the availability of labeled data for airport surveillance, a robust methodology is required to eliminate noise in the observations. Factors like, the proximity of objects due to the arbitrary distributions, visual similarity between structures, and the number of objects contribute majorly to the data variability in remote sensing images. Thus, requires enhanced techniques to tackle data variability. Non-uniform imaging environments also continue to increase the complexity of image-processing tasks.

It is observed that there is insufficient research on the quantification of images based on spatial heterogeneity and multi-scale multi-resolution. Therefore, it is crucial to identify approaches to enhance the selection of spatial scale for analyzing and differentiating aggregated data.

In the area of deep learning, a variety of convolutional neural networks (CNN) have aided in deep feature extractions to study the data variability in depth. The performance of image processing tasks have notably enhanced with the introduction of CNN's, which allows for model transferability and generalizations to describe the local semantics of an image. Although various qualitative assessments are widely used for performing remote sensing image processing, these rely heavily on scale sensitivity and expert knowledge for accurate and precise object representations. Therefore, the goal of our research is to develop a generic model applying different dynamic kernels. Furthermore, these models are designed to aid in quantitative assessments that help in determining the optimum scale range for object representations in remote sensing images. Kernel methods effectively preserve both the local and global structure in addition to handling high variations in patterns.

Researchers have proposed multiple kernel methods like the Base kernel function in dynamic kernels to enable similarity index measurement by calculating the proximity of the local features in an image. The posterior probability of local features corresponding to Gaussian Mixture Models (GMM) is calculated in the probability-based kernels. Kernel computations in matching base kernels restrain themselves to include features that are analogous to the mean of the GMM ensuring the retention of spatial patterns.

Taking inspiration from both deep learning techniques and machine learning methods, we propose a learning method to address the data variability and scale sensitivity in remote sensing images. Our approach consists of two critical phases – feature extraction and model training. Local features are extracted using CNN and then we train these features using a universal GMM. Both the local and global attributes are learned using the kernels for better representations. The variability in spatial patterns is handled by dynamic kernels. The similarity index is then calculated using the means of GMM and the distance between features in the images.

It is observed the use of kernel methods allows for combining different feature entities and dimensions to account for high dimensional data. Kernel methods achieve a better separability by projecting distances to higher dimensions, however, are identified to be most suitable for fixed-length pattern handling. This constrains the comparison between two images containing a varying number of local features. Hence, dynamic kernels are used in our approach which enables the transformation and assimilation of spatial variability in images.

The major contributions of the paper is as follows:

1. A generic Gaussian Mixture Model (GMM) is trained to learn the scale effect using three different scale views and objects from remote sensing images for better evaluation of scale sensitivity for learning representations.
2. Dynamic kernels are introduced to handle variations across scales and resolutions. The global variations are captured to preserve local structures while managing the spatial variability in object patterns.
3. The efficacy is demonstrated on a custom dataset that is developed using :
   (a) NWPU-RESIC45 (Cheng et al., 2017) – six classes, namely, airplane, building, freeway, parking lot, runway, and vehicles are considered. The spatial resolution of the images ranges from 0.2m to 30m.
   (b) Images captured from GoogleEarth™ for six object classes, namely, airplane, building, freeway, parking lot, runway, and vehicles. The images are captured at three different scales / resolutions –
      i. SS05 subset dataset - Scale - 1:500; Spatial Resolution : 0.125m
      ii. SS10 subset dataset - Scale - 1:1000; Spatial Resolution : 0.25m
      iii. SS20 subset dataset - Scale - 1:2000; Spatial Resolution : 0.5m

The remainder of this paper is organized as follows: the related research works on scale effects on remote images, classification tasks, and dynamic kernels are summarized in Section 2. The Section 3 describes the proposed approach to classify and identify the optimum range of object representations in remote sensing images using dynamic kernels. The experimental results along with the analysis are summarized in the Section 4. In Section 5 we provide the conclusion and future works of this paper.

2 RELATED WORKS

This section details about the existing works on image classifications, dynamic kernels usage in remote sensing image processing, and scale-effect analysis on remote sensing images in general and in the context of airport object representations.

2.1 Object Classifications in Remote Sensing Images

The initial research on object representation using remote sensing images indicates the handcrafted techniques to extract multi-level (low, mid, and high) features for object classifications.

Early works (Pi et al., 2003; Jackson et al., 2015; Cheng et al., 2017; Burghouts and Geusebroek, 2009; Geusebroek et al., 2001; Van De Sande et al., 2009) used handcrafted methods focusing on geometric characteristics, namely, shape, color, edge and boundary, texture, and structural information. The studies also indicate the use of statistical features, namely, variances, means, intensity, etc., to extract low-level features. These methods predominantly used local features and to some extent global features, however, local properties could not be encoded completely.

Later works (Yang and Newsam, 2008; Cheng et al., 2015a; Cheng et al., 2014; Cheng et al., 2015b; Cheng et al., 2015c) discuss the use of scale-invariant transform features, histogram of oriented gradients (HOG) features, and explored various representations. In more recent years, convolutional neural networks (CNN) is used for effective image classifications. These methods (Cheng et al., 2018; Akbar et al., 2019; He et al., 2018; Nogueira et al., 2017; Sitaula et al., 2020) allow for the extraction of low, mid, and high-level features providing a better representation of objects/scenes in remote sensing images. They also provide better generalization and transferability. However, we observe that there has been negligible work in object representation for airport surveillance. These methods allow to preserve the spatial information but fail to provide better discrimination during the training process.

2.2 Dynamic Kernels Usage in Remote Sensing Images

In recent years, we have observed the introduction of dynamic kernels in audio, image, video, and speech analysis in various domains. The dynamic kernels due to their ability to represent variable length patterns to fixed length patterns allow for better discrimination of data. An intermediate matching kernel (IMK) (Boughorbel et al., 2005) is developed to reduce computational complexity. A set of virtual feature vectors are used to obtain the nearest local feature vector. Methods like Gaussian densities are used to construct probabilistic sequence kernels and similarities are derived using distance-based measures (Lee et al., 2007; You et al., 2009). A universal background model is generated that models the features from various inputs and is trained. A mean super vector model is created that adapts the means and covariances of the universal model thus creating a kernel function. This kernel function called Gaussian means interval kernel (MIK) along with a support vector machine aids in the classification tasks.

These models are based on Gaussian mixture models and are deemed to be highly effective. More recently, (Datla et al., 2021) discusses the use of dynamic kernels for scene classifications using various dynamic kernel methods and support vector machine (SVM).

2.3 Scale-Effect Analysis in Remote Sensing Images

Early research has used several representative methods for scale effect analysis on remote sensing images, such as, Geographic variance method (GVM) (Moellering and Tobler, 1972), Wavelet transform method (WTM) (Pelgrum, 2000), Local variance method (LVM) (Woodcock and Strahler, 1987), Semi-variograms methods (Artan et al., 2000; Wackernagel, 1996; Garrigues et al., 2006), and Fractal methods. However, these methods relied on relative variability, strict dimensions for data sets, dependencies on mother wavelets, a global variance of images, etc. They introduce difficulties in comparing local variances and depends heavily on second-order hypothesis as well as irregularities of an object.

In later years, (Ming et al., 2015) in their work proposes scale selection based on spatial statistics for Geo-Object-Based Image Analysis(GEOBIA), using average local variance graph to replace semi-variograms to pre-estimate the optimal spatial bandwidth using segmentation. Average local variograms are suitable for local information extraction and fail to capture information from complex nested structures or scenes. These tasks are based on segmentation techniques and hence computationally expensive. Also, enhancements of algorithms to multi-spectral images become challenging.

From the existing literature, we observe that most of the research focused on classification tasks, scale-effect analysis, and/or dynamic kernel analysis in varied domains. There is limited work in airport object representations using one or a combination of the above-mentioned methods.

3 PROPOSED METHOD

In this section, we detail the proposed approach for identifying the optimum scale range for object representations in remote sensing images that will aid in better surveillance decision-making. Airport images are captured at different spatial resolutions and feature representations are learned using large Gaussian Mixture models (GMM). Dynamic kernel GMMs can handle the disparities due to scale variations and image capturing by effectively preserving the local structure information. These kernels are designed for varying length patterns extracted from image data that correspond to sets of local feature vectors. The entire process can be described in Figure 1 and consists of various stages, namely, data pre-processing feature extraction, Gaussian mixture model training and adaptation, feature representations using dynamic kernels, classification, and finally optimum scale range analysis.

3.1 Data Processing and Feature Extraction

One of the challenging areas for the application of computer vision-based algorithms to remote sensing images is scale variability. In our proposed method, images are obtained at various scales ranging from 1:500 to 1:2000 with a spatial resolution of 0.125m to 0.5m. Each of these images is resized to a one-size of 640×640 pixels. In addition, we introduce zero padding at the top/bottom or left/right for all non-square images to support batch processing and maintain aspect ratios.

The limited availability and the hyperspectral nature of remote sensing images make them statistically different from natural images, and hence difficult to extract relevant features for training. Based on recent advancements, the dataset is further enhanced using both transfer learning and data augmentation techniques. The images undergo color variations, horizontal flips, random θ rotation, resizing, translations, and vertical flips. We use convolutional neural networks to extract multi-level (low, mid, and high) features from remote sensing images along with transfer learning by fine-tuning the layers with pre-trained convolutional neural network models. Thus, enabling learning of generic features like those extracted using edge or line detectors. These features are fed to the Gaussian mixture model in the training phase to compute various statistics that allow for a quantitative evaluation of the geographical variability.

3.2 Training the Gaussian Mixture Model (GMM)

The features extracted from the convolutional neural networks are used to train the Gaussian mixture model (GMM). Given an image, each sample of the image can be represented as I, the set of feature vectors are represented as $\mathbf{i}_1, \mathbf{i}_2, \mathbf{i}_3 \dots \mathbf{i}_N$, where N is the total number of local features extracted for the given image I. The Gaussian mixture parameters is determined based on the probability of occurrence of the latent variable z, and can be defined as in Eqn. (1), which is actually equivalent to mixing the coefficient for that Gaussian.

$$\pi_k = p(z_k = 1) \tag{1}$$

The likelihood of the particular feature $\mathbf{i}_n$ generated from the GMM model for $\mathbf{z} = \{z_1, z_2, ..., z_K\}$ is given by Eqn. (2)

$$p(\mathbf{i}_n) = \sum_{k=1}^{K} p(i_n|z)p(z) = \sum_{k=1}^{K} \pi_k \mathcal{N}(i_n|\mu_k, \Sigma_k) \tag{2}$$

where, k indicates each of the GMM component, K is the total number of GMM components, μ_k, σ_k represents the mean and the covariance respectively. The Gaussian mixture weights is given by π_k that satisfies the constraint $\sum_{k=1}^{K} \pi_k = 1$. The optimal values are determined using the Expectation-Maximization algorithm, which is an iterative method to identify the parameters $\theta = \{\pi,\ \mu,\ \Sigma\}$ for fitting the mixture of Gaussian models generated.

The Expectation-Maximization algorithm can be divided into 2 steps, namely, the E-step and the M-Step. In the Expectation step, we initialize and continue to estimate the value of missing variables by calculating the probability of the data point $\mathbf{i}_n$ belonging

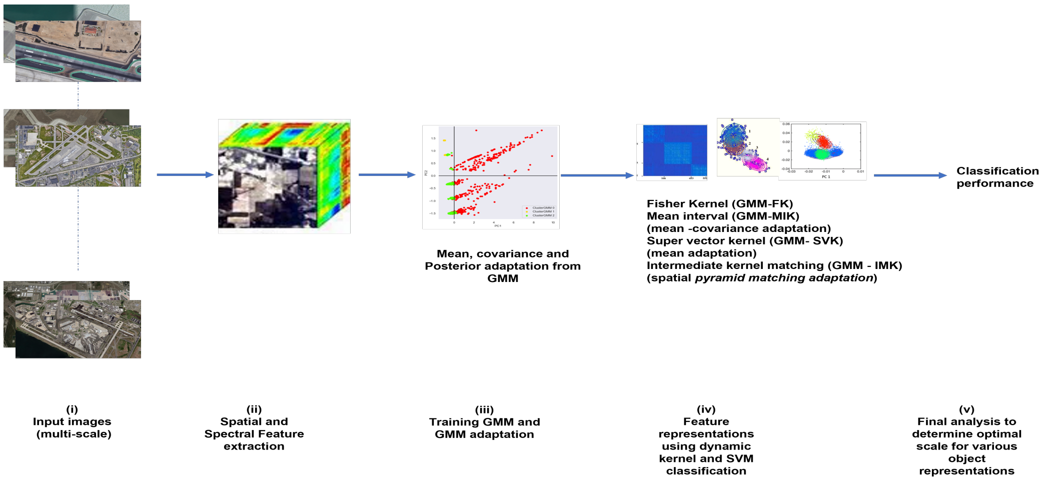

Figure 1: Block diagram for the proposed method to find the optimum scale range for object representations using dynamic kernels for Airport surveillance.

to distribution **z**. In the Maximization step, the parameters θ is updated using the values estimated in the previous step.

The attributes and the variances in the spatial patterns are captured in the Gaussian components after the training phase. This helps in comparing the different images improving intra-class variability. Each of the feature vectors $\mathbf{i}_n$ is aligned to the k^{th} component of the Gaussian mixture model using the posterior probabilities and is defined as in Eqn. (3).

$$p(k|\mathbf{i}_n) = \frac{\pi_k p(\mathbf{i}_n|k)}{\sum_{k=1}^{K} \pi_k p(\mathbf{i}_n|k)} \tag{3}$$

The *maximum aposteriori* (MAP) adaptation helps in generating multiple dynamic kernel-based representations, that can efficiently represent each of the images. These representations are further detailed in the subsequent sections.

3.3 Feature Representations Using Dynamic Kernels

Identifying the right kernel function for feature representations is critical to obtain a good performance. In the earlier days, multiple kernel functions are developed for the static or fixed-length pattern. In recent years, researchers have discussed the dynamic kernels built to address variable length patterns by designing a new kernel function or converting the variable length to fixed length patterns. In this section, we detail the various dynamic kernel functions that effectively preserve both local and global information for better feature representations.

3.3.1 Mapping Based Dynamic Kernel

This method uses a Gaussian mixture model-based likelihood to explicitly map a set of variable length representations onto a fixed dimensional representation. To obtain the maximum likelihood estimate of the parameter θ, we calculate the derivative or gradient of the log-likelihood function defined in Eqn. (3) for a given image **I**. The first derivatives of mean, covariance, and weight parameters are defined as in Eqn. (4), Eqn. (5), and Eqn. (6), respectively.

$$\psi_k^{(\mu)}(\mathbf{I}) = \sum_{j=1}^{J} p(k|\mathbf{i}_j)\mathbf{r}_{jk}, \tag{4}$$

$$\psi_k^{(\sigma)}(\mathbf{I}) = \frac{1}{2}\left(\sum_{j=1}^{J} p(k|\mathbf{i}_j)\left[-(\mathbf{x}_k)+\mathbf{y}_{jk}\right]\right), \tag{5}$$

$$\psi_k^{(\pi)}(\mathbf{I}) = \sum_{j=1}^{J} p(k|\mathbf{i}_j)\left[\frac{1}{\pi_k} - \frac{p(k_1|\mathbf{i}_j)}{\pi_1 p(k|\mathbf{i}_j)}\right] \tag{6}$$

where, $\mathbf{r}_{jk} = \Sigma_k^{-1}(\mathbf{i}_j - \mu_k)$, $\mathbf{x}_k = \Sigma_k^{-1}$, $\mathbf{y}_{jk} = [r_{j1k}\mathbf{r}_{jk}^T, r_{j2k}\mathbf{r}_{jk}^T, \ldots, r_{jdk}\mathbf{r}_{jdk}^T]$ for any $d \times d$ matrix **A** with elements $a_{ij}, i, j = 1, 2, \ldots, d$ and $vec(\mathbf{A}) = [a_{11}, a_{12}, \ldots, a_{dd}]$.

The Eqn. (4), Eqn. (5), and Eqn. (6) determines the direction of the parameters (μ, σ, π). These gradients are updated to obtain the best fit of the model. The gradients capture the deviations introduced in the objects due to spatial variability. The Fisher score vector, which is the fixed dimensional feature vector is computed by stacking the gradients from the Eqn. (4), Eqn. (5), and Eqn. (6).

$$\phi_k(\mathbf{I}) = \left[\psi_k^{(\mu)}(\mathbf{I})^T, \psi_k^{(\sigma)}(\mathbf{I})^T, \psi_k^{(\pi)}(\mathbf{I})^T\right]^T \tag{7}$$

The Fisher score vector, for all the **K** components of the GMM for a given space s, is given by the Eqn. (8).

$$\phi_s(\mathbf{I}) = \left[\phi_1(\mathbf{I})^T \phi_2(\mathbf{I})^T \phi_K(\mathbf{I})^T\right]^T \tag{8}$$

The similarities between the two samples I_u and I_v with given local features, is captured by the Fisher score vector and the kernel function is given by the Eqn. (9).

$$\mathbf{K}_{FK}(\mathbf{I}_u, \mathbf{I}_v) = \phi_s(\mathbf{I}_u)^T \mathbf{F}^{-1} \phi_s(\mathbf{I}_v) \tag{9}$$

where **F** is the Fisher information matrix which is the covariance in the Mahanolibis distance and is given by the Eqn. (10).

$$\mathbf{F} = \frac{1}{D} \sum_{d=1}^{D} \phi_s(\mathbf{I}_d) \phi_s(\mathbf{I}_d)^T \tag{10}$$

The spatial variability between two image samples is captured in the Fisher information matrix. Fisher score and Fisher information matrix, thus capture both the local and global information in the Fisher kernel computation. However, the Fisher Kernel approach is computationally expensive.

3.3.2 Probability Based Kernel Functions

The probability-based kernel functions compare the probability distribution of the local feature vectors of two images. In this method, the set of variable length local feature representations are mapped onto fixed dimensional feature representations in the kernel space using the probabilities. The *maximum aposterior* (MAP) adaptation of mean and covariances are calculated as given in the Eqn. (11a) and Eqn. (11b), respectively.

$$\mu_k(\mathbf{I}) = \alpha \mathbf{F}_k + (1-\alpha)\mu_k, \tag{11a}$$

$$\sigma_k(\mathbf{I}) = \alpha \mathbf{S}_k(\mathbf{I}) + (1-\alpha)\sigma_k \tag{11b}$$

where $\mathbf{F}_k$ and $\mathbf{S}_k$ are the first and second-order Baum-Welch statistics for an image **I**, respectively, and is calculated as in Eqn. (12a) and Eqn. (12b), respectively.

$$\mathbf{F}_k(\mathbf{I}) = \frac{1}{m_k(\mathbf{I})} \sum_{m=1}^{M} p(k|i_m) i_m, \tag{12a}$$

$$\mathbf{S}_k(\mathbf{I}) = diag\left(\sum_{m=1}^{M} p(k|i_m) i_m i_m^T)\right) \tag{12b}$$

The posterior probabilities of the given GMM component for each of the image samples are determined by the adapted mean and covariance. It is also observed that the posterior probabilities are directly dependent on the adapted mean and covariance, implying, that the higher the probability higher is the correlation among the features captured in the GMM components. Thus, indicating that the adapted mean and covariances have a higher impact than the original full GMM mean and covariance. We further derive the GMM vector $\psi_k(\mathbf{I})$ for an image **I** as in Eqn. (13).

$$\psi_k(\mathbf{I}) = \left[\sqrt{\pi_k} \sigma_k^{\frac{-1}{2}} \mu_k(\mathbf{I})\right]^T \tag{13}$$

The GMM super vector (GMM-SV) and the super vector kernel $\mathbf{S}_{svk}(\mathbf{I})$ and $\mathbf{K}_{svk}(\mathbf{I}_u, \mathbf{I}_y)$ as defined in Eqn. (14a) and Eqn. (14b), respectively, is obtained by stacking the GMM vector for each component. We obtain a supervector of $Kd \times 1$ dimension that utilizes the first order adaptations.

$$\mathbf{S}_{svk}(\mathbf{I}) = \left[\psi_1(\mathbf{I})^T, \psi_2(\mathbf{I})^T, ..., \psi_K(\mathbf{I})^T\right]^T, \tag{14a}$$

$$K_{SVK}(\mathbf{I}_u, \mathbf{I}_v) = \mathbf{S}_{svk}(\mathbf{I}_u)^T \mathbf{S}_{svk}(\mathbf{I}_v) \tag{14b}$$

In the super vector kernel method, we only utilize first order statistics of the GMM. To obtain the mean interval vector for every component k of the GMM, the second order statistics and the adapted means is used as in Eqn. (15a). This help determine the statistical dissimilarities between the mean and covariance of the mean interval vector. The GMM mean interval supervector is created by combining the mean interval vectors across GMM mixtures $\mathbf{S}_{mik}$ and the associated GMM mean interval kernel $\mathbf{K}_{MIK}$ between two images $\mathbf{I}_u$ and $\mathbf{I}_v$ and is as given by Eqn. (15b) and Eqn. (15c), respectively.

$$\psi_k(\mathbf{I}) = \left(\frac{\sigma_k(\mathbf{I}) - \sigma_k}{2}\right)^{\frac{-1}{2}} (\mu_k(\mathbf{I}) - \mu_k) \tag{15a}$$

$$\mathbf{S}_{mik}(\mathbf{I}) = \left[\psi_1(\mathbf{I})^T, \psi_2(\mathbf{I})^T, ...\psi_K(\mathbf{I})^T\right]^T \tag{15b}$$

$$\mathbf{K}_{MIK}(\mathbf{I}_u, \mathbf{I}_y) = \mathbf{S}_{mik}(\mathbf{I}_u)^T \mathbf{S}_{mik}(\mathbf{I}_v) \tag{15c}$$

3.3.3 Matching Based Kernel Functions

The mapping-based and probability-based kernel methods are based on mapping the feature representations from a variable to a fixed length. An alternate method to handle variable data lengths also known as matching-based kernels is introduced in this section. In this method, a pair of images is matched using their local features (Datla et al., 2021) vectors. We use an intermediate matching kernel (IMK) function that is calculated using both the local feature vector and the virtual feature vector. The virtual feature vectors are obtained using the training data and are the closest match to a set of local features. The feature vectors i^*_{ul} and i^*_{vl} in $\mathbf{I}_u$ and $\mathbf{I}_v$ closest to the l^{th} virtual feature vector $\mathbf{q}_l$ is given by the Eqn. (16).

$$\mathbf{i}^*_{ul} = \underset{i \in \mathbf{I}_u}{arg\ min}\ \mathcal{D}(\mathbf{i}, \mathbf{q}_l)\ and\ \mathbf{i}^*_{vl} = \underset{i \in \mathbf{I}_v}{arg\ min}\ \mathcal{D}(\mathbf{i}, \mathbf{q}_l) \tag{16}$$

where $\mathbf{Q} = \{\mathbf{q}_1, \mathbf{q}_2, \ldots \mathbf{q}_L\}$ represents the virtual feature vectors and $\mathcal{D}(.,.)$ measures the distance between the feature vectors $\mathbf{I}_u$ or $\mathbf{I}_v$ from the nearest feature vector in $\mathbf{Q}$. The distance function helps in identifying the closest matching point and hence the spatial distance learned from one image to another, which is captured by the GMM components. The kernel function $\mathbf{K}_{IMK}$ is given by Eqn. (17).

$$\mathbf{K}_{IMK}(\mathbf{I}_u, \mathbf{I}_v) = \sum_{l=1}^{L} k(\mathbf{i}_{ul}, \mathbf{i}_{vl}) \tag{17}$$

The set of virtual feature vectors also includes the mean, covariance, and the weights. The posterior probability of the GMM component determines the distance, thus computing the virtual feature vectors i^*_{ul} and i^*_{vl} for a given l for the image samples $\mathbf{I}_u$ or $\mathbf{I}_v$ as in Eqn. (18).

$$\mathbf{i}^*_{ul} = \underset{i \in \mathbf{I}_u}{arg\ max}\ p(l|\mathbf{i})\ and\ \mathbf{i}^*_{vl} = \underset{i \in \mathbf{I}_v}{arg\ max}\ p(l|\mathbf{i}) \tag{18}$$

3.4 Classification and Optimum Scale Range Analysis

In the next phase, we implement the Support Vector Machine (SVM) for the classification task, for each of the dynamic kernels. The support vector algorithm helps determine a hyperplane between different classes. Based on the dynamic kernel function selected, we maximize the separation boundaries between the data points. For multi-class classification, we use the one vs. all approach to find the hyperplane to separate the classes. We use N support vector machines to classify data points from N class data sets. For R training samples $(I_r, y_r)_{r=1}^{R}$, where the label for a particular class is represented by y_r and the discriminant function is given by the Eqn. (19),

$$f(I) = \sum_{r=1}^{R} \alpha^*_r y_r K_{DK}(I, I_r) + bias^* \tag{19}$$

where R_s represents the number of support vectors, the optimal values of the Lagrangian coefficient is given by α^* and $bias^*$ represents the optimal bias. The class of I is determined by the sign of the function f. The 10-fold cross-validation helps discriminate the sample of the particular class against all other classes. Further, we determine the correlation values for various classes at different spatial distances. This helps determine optimal range for the object representations.

4 EXPERIMENTAL RESULTS AND ANALYSIS

The objective of our method is to identify the optimum scale range for object representations that aids in better airport surveillance. In this section, we discuss in detail the experimental results of applying various dynamic kernel functions, namely, mapping based, probability based and matching based kernels on our custom dataset.

4.1 Datasets and Environmental Setup

Vision-based airport surveillance is challenging due to non-availability of appropriate datasets. The commonly available remote sensing dataset is the NWPU-RESISC45 (Cheng et al., 2017) that is design for the classification tasks. This dataset consists of 45 scenes with a mix of 31,500 images with spatial range of 0.2m to 30m. The images are sized to 256 × 256 pixels each. These images fail to provide the relevant statistics based on the spatial distance.

Therefore, a custom dataset is developed by capturing images from NWPU-RESISC45 (Cheng et al., 2017), different public repositories and from GoogleEarth™ at different spatial resolutions - 0.125m (Scale - 1:500), 0.25m (Scale - 1:1000), and 0.5m (Scale - 1:2000) to obtain a realistic view of the dataset. The final airport object dataset is created with six object categories, namely, vehicles, airplanes, runway, building, freeway, and parking lot.

The sample dataset is as shown in Figure 2. The objects of interest are labeled using the polygon annotation. A bounding box (x_1, y_1, x_2, y_2) is drawn using the polygon points where (x_1, y_1) and (x_2, y_2) represents the top-left and bottom-right coordinates using manual process and AI-enabled annotation tool.

The model is implemented using an NVIDIA GeForce RTX 2060 Super EX (1-Click OC) with CUDA cores 2176 and an 8GB GDDR6 256-bit DP/HDMI. The proposed method is developed using

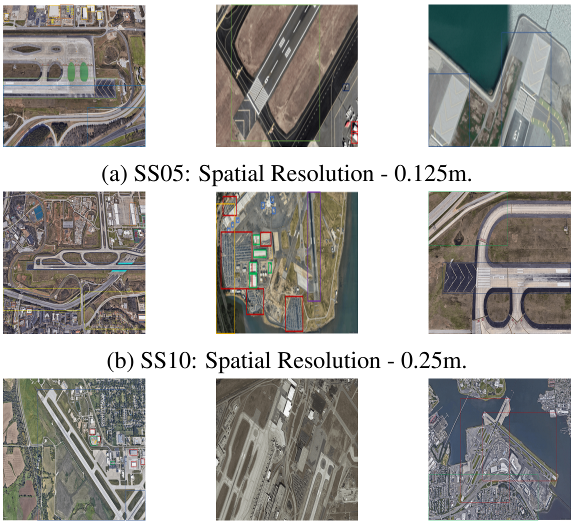

(a) SS05: Spatial Resolution - 0.125m.

(b) SS10: Spatial Resolution - 0.25m.

(c) SS20: Spatial Resolution - 0.5m.

Figure 2: Airport Object Dataset: (a) SS05 : Spatial Resolution - 0.125m (b) SS10 : Spatial Resolution - 0.25m (c) SS20: Spatial Resolution - 0.5m.

open-source frameworks Keras, OpenCV, and TensorFlow.

We use different convolutional features of various convolutional neural networks (CNNs), namely, AlexNet (Krizhevsky et al.,), GoogLeNet (Szegedy et al., 2015), VGGNet-16 (Simonyan and Zisserman, 2014), DenseNet-121 (Huang et al., 2017), ResNet-50 (He et al., 2016), and EfficientNet-B0 (Tan and Le, 2019) as shown in Table 1 for extraction of both local and global feature vectors for GMM training. We train a total of 24 GMMs, i.e, features from six convolutional neural network models for four mixtures on three dataset combinations from the custom dataset.

Table 1: Feature map sizes of various CNN Architectures used for object representation modeling.

Architecture	Feature Layer	Feature Map Size
AlexNet	$conv5$	$13 \times 13 \times 256$
GoogLeNet	$inception\ 4(e)$	$14 \times 14 \times 832$
VGGNet-16	$block5\_conv3$	$13 \times 13 \times 256$
DenseNet-121	$conv4\_block16$	$7 \times 7 \times 1024$
ResNet-50	$conv5\_block4$	$7 \times 7 \times 2048$
EfficientNet-B0	top_conv	$7 \times 7 \times 1280$

4.2 Dynamic Kernel Evaluations

The performance of various dynamic kernels on our custom dataset that is distributed based on the spatial resolutions 1:500, 1:1000, and 1:2000 is as shown in Table 2, Table 3, and Table 4, respectively. The classification performance is evaluated using support vector machine. The experimental results indicate that the performance is best observed with the features extracted using EfficientNet-B0 followed by ResNet-50 and DenseNet-121 for different GMM mixtures and datasets. We also observe that as the number of components increases, the accuracy comes to a close saturation. As shown in the Table 2, Table 3, and Table 4, for a GMM mixture with 128 components, the accuracy is less as compared to that of 64 component. The results also indicate that classification performance is better with supervector kernels (GMM-SVK) and mean interval kernels (GMM-MIK) compared to the fisher kernel (GMM-FK) and intermediate matching kernel (GMM-IMK).

4.3 Scale Effect Analysis

The scale-effect analysis is evaluated by measuring the Pearson correlation coefficient. The input features provide insight into the relationships between different object classes for each of the subset datasets SS05, SS10, and SS20.

SS05 dataset: The best classification accuracy of 96.89% is achieved for 128 components using GMM-MIK as shown in Table 2. From the Figure 3a, at a scale of 0.125m, we observe the following:

- High correlation between freeway and runways,
- Vehicles have a high correlation with buildings and parking lots.
- Airplanes are best classified at this range due to low correlations.

SS10 dataset: The best classification accuracy of 97.65% is achieved for 64 components using GMM -MIK as shown in Table 3. From Figure 3b, at a scale of 0.25m, we observe that all objects are less correlated and better classified.

*SS20 dataset:*The best classification accuracy of 95.32% is achieved for 64 components using GMM-MIK as shown in Table 4. From Figure 3c, at a scale of 0.5m, we observe that there is at least one pair of objects highly correlated which makes the classification tasks difficult to achieve.

Table 2: Classification accuracy (%) of various GMMS- GMM-FK, GMM-SVK, GMM-MIK, GMM-IMK over GMM mixtures on SS05 subset dataset.

CNN Model			**AlexNet**	**GoogLeNet**	**VGGNet-16**	**DenseNet-121**	**ResNet-50**	**EfficientNet-50**
GMM -FK	# GMM Mixtures	16	45.42	48.21	47.63	51.28	40.53	44.32
		32	48.34	48.18	48.72	54.63	51.74	55.45
		64	47.91	48.61	49.51	53.45	52.87	56.73
		128	47.66	48.98	49.45	52.55	51.46	54.83
GMM -SVK	# GMM Mixtures	16	81.65	82.47	88.69	90.35	94.27	95.32
		32	82.41	83.49	88.72	94.53	95.43	96.37
		64	84.32	86.33	89.25	94.82	95.65	95.41
		128	84.66	87.29	89.86	96.76	95.23	96.34
GMM -MIK	# GMM Mixtures	16	78.26	80.24	81.23	91.92	93.43	94.56
		32	79.32	79.27	83.46	88.72	92.35	96.73
		64	79.17	81.54	83.91	94.97	95.27	95.23
		128	78.93	82.34	82.68	93.28	95.66	**96.89**
GMM -IMK	# GMM Mixtures	16	62.57	67.14	69.23	74.18	66.17	75.12
		32	62.49	69.2	69.56	75.22	75.67	76.45
		64	64.18	69.46	69.64	74.76	76.34	77.45
		128	66.62	68.87	69.25	75.33	76.2	77.28

Table 3: Classification accuracy (%) of various GMMS- GMM-FK, GMM-SVK, GMM-MIK, GMM-IMK over GMM mixtures on SS10 subset dataset.

CNN Model			**AlexNet**	**GoogLeNet**	**VGGNet-16**	**DenseNet-121**	**ResNet-50**	**EfficientNet-50**
GMM -FK	# GMM Mixtures	16	47.35	51.76	52.63	52.35	51.33	55.21
		32	47.76	53.23	51.25	63.43	61.65	65.78
		64	46.34	51.34	52.45	64.57	63.56	66.24
		128	48.66	52.54	51.23	64.23	62.49	65.32
GMM -SVK	# GMM Mixtures	16	77.26	83.36	83.56	92.23	94.76	95.12
		32	78.87	81.34	81.56	94.34	93.67	95.45
		64	78.32	82.75	82.78	94.23	94.98	96.89
		128	79.24	83.24	83.23	93.22	94.32	96.32
GMM -MIK	# GMM Mixtures	16	80.34	86.56	87.54	91.76	95.19	95.32
		32	82.67	85.45	87.65	92.99	94.8	97.32
		64	83.87	85.65	88.34	95.87	95.34	**97.65**
		128	83.44	87.65	87.25	95.92	95.67	95.36
GMM -IMK	# GMM Mixtures	16	66.36	65.56	68.65	75.43	75.34	75.33
		32	69.39	68.56	67.34	76.34	76.36	76.76
		64	68.38	69.34	66.78	76.23	77.1	77.98
		128	67.56	69.34	68.43	76.76	77.14	77.65

Table 4: Classification accuracy (%) of various GMMS- GMM-FK, GMM-SVK, GMM-MIK, GMM-IMK over GMM mixtures on SS20 subset dataset.

CNN Model			**AlexNet**	**GoogLeNet**	**VGGNet-16**	**DenseNet-121**	**ResNet-50**	**EfficientNet-50**
GMM -FK	# GMM Mixtures	16	45.35	47.62	47.12	51.33	58.45	59.23
		32	48.77	57.92	57.34	52.34	59.25	59.43
		64	49.54	47.45	48.34	51.76	58.14	53.42
		128	40.23	47.87	48.23	53.34	52.45	51.78
GMM -SVK	# GMM Mixtures	16	76.65	79.35	79.13	83.16	89.98	93.87
		32	78.24	80.23	80.21	84.33	90.24	94.23
		64	76.33	80.87	81.22	85.45	91.34	94.85
		128	76.65	84.32	81.45	86.13	92.42	94.44
GMM -MIK	# GMM Mixtures	16	79.82	83.56	83.32	85.66	92.32	95.28
		32	80.34	84.21	84.55	85.34	93.56	95.18
		64	81.52	85.43	84.78	86.67	93.38	**95.32**
		128	80.11	85.92	85.34	86.89	94.56	95.28
GMM -IMK	# GMM Mixtures	16	66.54	76.23	73.34	76.54	85.87	85.43
		32	68.65	75.36	73.67	76.78	85.92	85.16
		64	69.32	75.32	74.34	77.43	85.45	86.56
		128	69.45	75.56	74.87	77.29	86.34	84.29

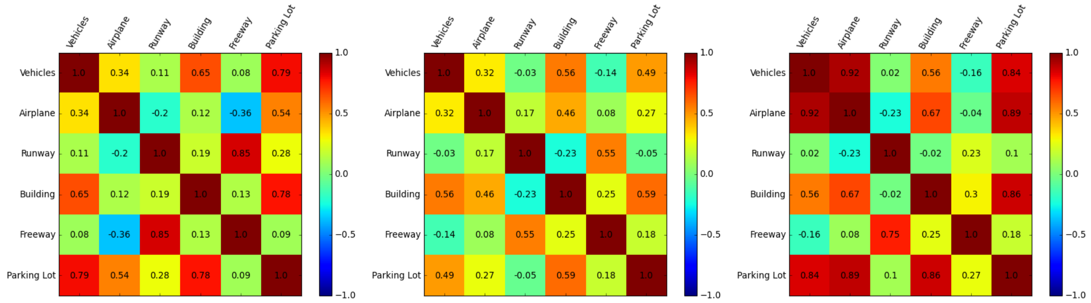

(a) SS05 subset dataset. (b) SS10 subset dataset. (c) SS20 subset dataset.

Figure 3: Correlation matrix of GMM-MIK for (a) SS05 subset dataset (b) SS10 subset dataset (c) SS20 subset dataset.

5 CONCLUSIONS

In this work, we introduce the use of dynamic kernels to find the optimum scale range for object representations in remote-sensing images. For this, we exploit multiple dynamic kernels, namely, Fisher Kernel (GMM-FK), Intermediate Matching Kernel (GMM-IMK), Mean Interval Kernel (GMM-MIK), and Super Vector Kernel (GMM-SVK) methods. The scale effect analysis is evaluated using the first- and second-order statistics of the Gaussian mixture model. The Gaussian mixture models allow capturing spatial and object variability while continuing to preserve the global variance. Our analysis indicates that the mean interval kernel method (GMM-MIK) is most suitable for the classification task. We introduce a custom dataset consisting of images at different spatial ranges to evaluate the performance of our method. In the future, the method needs to be optimized to find a closer range of optimum values for object representations. The method also needs to be expanded to evaluate additional object classes to reflect the real-time environment.

REFERENCES

Akbar, J., Shahzad, M., Malik, M. I., Ul-Hasan, A., and Shafait, F. (2019). Runway detection and localization in aerial images using deep learning. In *2019 Digital Image Computing: Techniques and Applications (DICTA)*, pages 1–8. IEEE.

Artan, G. A., Neale, C. M., and Tarboton, D. G. (2000). Characteristic length scale of input data in distributed models: implications for modeling grid size. *Journal of Hydrology*, 227(1-4):128–139.

Boughorbel, S., Tarel, J. P., and Boujemaa, N. (2005). The intermediate matching kernel for image local features. In *Proceedings. 2005 IEEE International Joint Conference on Neural Networks, 2005.*, volume 2, pages 889–894. IEEE.

Burghouts, G. J. and Geusebroek, J.-M. (2009). Performance evaluation of local colour invariants. *Computer Vision and Image Understanding*, 113(1):48–62.

Cheng, G., Han, J., Guo, L., and Liu, T. (2015a). Learning coarse-to-fine sparselets for efficient object detection and scene classification. In *Proceedings of the IEEE conference on computer vision and pattern recognition*, pages 1173–1181.

Cheng, G., Han, J., Guo, L., Liu, Z., Bu, S., and Ren, J. (2015b). Effective and efficient midlevel visual elements-oriented land-use classification using vhr remote sensing images. *IEEE Transactions on Geoscience and Remote Sensing*, 53(8):4238–4249.

Cheng, G., Han, J., and Lu, X. (2017). Remote sensing image scene classification: Benchmark and state of the art. *Proceedings of the IEEE*, 105(10):1865–1883.

Cheng, G., Han, J., Zhou, P., and Guo, L. (2014). Multiclass geospatial object detection and geographic image classification based on collection of part detectors. *ISPRS Journal of Photogrammetry and Remote Sensing*, 98:119–132.

Cheng, G., Yang, C., Yao, X., Guo, L., and Han, J. (2018). When deep learning meets metric learning: Remote sensing image scene classification via learning discriminative cnns. *IEEE transactions on geoscience and remote sensing*, 56(5):2811–2821.

Cheng, G., Zhou, P., Han, J., Guo, L., and Han, J. (2015c). Auto-encoder-based shared mid-level visual dictionary learning for scene classification using very high resolution remote sensing images. *IET Computer Vision*, 9(5):639–647.

Datla, R., Chalavadi, V., et al. (2021). Scene classification in remote sensing images using dynamic kernels. In *2021 International Joint Conference on Neural Networks (IJCNN)*, pages 1–8. IEEE.

Garrigues, S., Allard, D., Baret, F., and Weiss, M. (2006). Quantifying spatial heterogeneity at the landscape scale using variogram models. *Remote sensing of environment*, 103(1):81–96.

Geusebroek, J.-M., Van den Boomgaard, R., Smeulders, A. W. M., and Geerts, H. (2001). Color invariance. *IEEE Transactions on Pattern analysis and machine intelligence*, 23(12):1338–1350.

He, K., Zhang, X., Ren, S., and Sun, J. (2016). Deep residual learning for image recognition. In *Proceedings of the IEEE conference on computer vision and pattern recognition*, pages 770–778.

He, N., Fang, L., Li, S., Plaza, A., and Plaza, J. (2018). Remote sensing scene classification using multilayer stacked covariance pooling. *IEEE Transactions on Geoscience and Remote Sensing*, 56(12):6899–6910.

Huang, G., Liu, Z., Van Der Maaten, L., and Weinberger, K. Q. (2017). Densely connected convolutional networks. In *Proceedings of the IEEE conference on computer vision and pattern recognition*, pages 4700–4708.

Jackson, P. T., Nelson, C. J., Schiefele, J., and Obara, B. (2015). Runway detection in high resolution remote sensing data. In *2015 9th International Symposium on Image and Signal Processing and Analysis (ISPA)*, pages 170–175. IEEE.

Krizhevsky, A., Sutskever, I., and Hinton, G. E. Imagenet classification with deep convolutional neural networks (alexnet) imagenet classification with deep convolutional neural networks (alexnet) imagenet classification with deep convolutional neural networks.

Lee, K.-A., You, C., Li, H., and Kinnunen, T. (2007). A gmm-based probabilistic sequence kernel for speaker verification. In *Eighth Annual Conference of the International Speech Communication Association*. Citeseer.

Ming, D., Li, J., Wang, J., and Zhang, M. (2015). Scale parameter selection by spatial statistics for geobia: Using mean-shift based multi-scale segmentation as an example. *ISPRS Journal of Photogrammetry and Remote Sensing*, 106:28–41.

Moellering, H. and Tobler, W. (1972). Geographical variances. *Geographical analysis*, 4(1):34–50.

Nogueira, K., Penatti, O. A., and Dos Santos, J. A. (2017). Towards better exploiting convolutional neural networks for remote sensing scene classification. *Pattern Recognition*, 61:539–556.

Pelgrum, H. (2000). *Spatial aggregation of land surface characteristics: impact of resolution of remote sensing data on land surface modelling*. Wageningen University and Research.

Pi, Y., Fan, L., and Yang, X. (2003). Airport detection and runway recognition in sar images. In *IGARSS 2003. 2003 IEEE International Geoscience and Remote Sensing Symposium. Proceedings (IEEE Cat. No. 03CH37477)*, volume 6, pages 4007–4009. IEEE.

Simonyan, K. and Zisserman, A. (2014). Very deep convolutional networks for large-scale image recognition. *arXiv preprint arXiv:1409.1556*.

Sitaula, C., Xiang, Y., Basnet, A., Aryal, S., and Lu, X. (2020). Hdf: Hybrid deep features for scene image representation. In *2020 International Joint Conference on Neural Networks (IJCNN)*, pages 1–8. IEEE.

Szegedy, C., Liu, W., Jia, Y., Sermanet, P., Reed, S., Anguelov, D., Erhan, D., Vanhoucke, V., and Rabinovich, A. (2015). Going deeper with convolutions. In *Proceedings of the IEEE conference on computer vision and pattern recognition*, pages 1–9.

Tan, M. and Le, Q. (2019). Efficientnet: Rethinking model scaling for convolutional neural networks. In *International conference on machine learning*, pages 6105–6114. PMLR.

Van De Sande, K., Gevers, T., and Snoek, C. (2009). Evaluating color descriptors for object and scene recognition. *IEEE transactions on pattern analysis and machine intelligence*, 32(9):1582–1596.

Wackernagel, H. (1996). Multivariate geostatistics: an introduction with applications. In *International Journal of Rock Mechanics and Mining Sciences and Geomechanics Abstracts*, volume 8, page 363A.

Woodcock, C. E. and Strahler, A. H. (1987). The factor of scale in remote sensing. *Remote sensing of Environment*, 21(3):311–332.

Yang, Y. and Newsam, S. (2008). Comparing sift descriptors and gabor texture features for classification of remote sensed imagery. In *2008 15th IEEE international conference on image processing*, pages 1852–1855. IEEE.

You, C. H., Lee, K. A., and Li, H. (2009). Gmm-svm kernel with a bhattacharyya-based distance for speaker recognition. *IEEE Transactions on Audio, Speech, and Language Processing*, 18(6):1300–1312.